Article

A Novel MPPT Control Method of Thermoelectric Power Generation with Single Sensor

Hiroaki Yamada [1],*, Koji Kimura [1], Tsuyoshi Hanamoto [1], Toshihiko Ishiyama [2], Tadashi Sakaguchi [2] and Tsuyoshi Takahashi [2]

[1] Kyushu Institute of Technology, 2-4, Hibikino, Wakamatsu, Kitakyushu, Fukuoka 808-0196, Japan; E-Mails: kimura-koji@edu.life.kyutech.ac.jp (K.K.); hanamoto@life.kyutech.ac.jp (T.H.)

[2] Kushiro National College of Technology, 2-32-1, Otanoshike, Kushiro, Hokkaido 084-0916, Japan; E-Mails: t-ishiyama@kushiro-ct.ac.jp (T.I.); sakaguti@kushiro-ct.ac.jp (T.S.); t-takahashi@kushiro-ct.ac.jp (T.T.)

* Author to whom correspondence should be addressed; E-Mail: hiroaki-ymd@life.kyutech.ac.jp; Tel.: +81-93-695-6043; Fax: +81-93-695-6043.

Abstract: This paper proposes a novel Maximum Power Point Tracking (MPPT) control method of thermoelectric power generation for the constant load. This paper reveals the characteristics and the internal resistance of thermoelectric power module (TM). Analyzing the thermoelectric power generation system with boost chopper by state space averaging method, the output voltage and current of TM are estimated by with only single current sensor. The proposed method can seek without calculating the output power of TM in this proposed method. The basic principle of the proposed MPPT control method is discussed, and then confirmed by digital computer simulation using PSIM. Simulation results demonstrate that the output voltage can track the maximum power point voltage by the proposed MPPT control method. The generated power of the TM is 0.36 W when the temperature difference is 35 °C. This is well accorded with the V-P characteristics.

1. Introduction

Currently attention is focusing on the energy harvesting technologies to electrify the small-rated electric devices by environmental energy such as waste heat energy and machine vibration. One of the power generation methods by waste heat energy is the thermoelectric power generation by Seebeck effect of thermoelectric power module (TM) [1]. The TM can generate the electric power at low-temperature difference. However the thermoelectric power generation has some problems, such as the energy conversion efficiency, thermal leakage, and internal resistance. It is necessary to improve the energy conversion efficiency from thermal energy to electric energy, to suppress the thermal leakage and to track the maximum power point voltage of TM.

We have proposed a method of suppressing the thermal leakage using heat pipes. The heat pipes were used for heat transfer from TM to heat sink avoiding thermal leakage. We confirmed to supply the electric power to the self-contained wireless telemetry by using the heat pipes and boost converter continuously. However, the boost converter controlled the output voltage of TM only. In [2,3], the impedance was mismatch between the TM and load impedance, so TM did not generate the maximum power. Thus, the maximum power point tracking (MPPT) control is necessary to maximize the power generation.

One of the MPPT control methods is the hill-climbing method, which is employed to seek the maximum power point by calculating the power with a voltage and current sensors [4]. This method needs two sensors to calculate and track the maximum power. We have proposed a method of the MPPT controller for TM by temperature detection [5]. The thermoelectric power generation system has been used for the power source of self-contained wireless telemetry. The reference output voltage of the TM is decided by the approximation formula of the V-P characteristics and the module temperature. This means the operation algorithm is simple, thus the one-chip microcomputer is enough to control the MPPT. The experimental results exhibit that the MPPT controller can track the maximum power point voltage. And then, the thermoelectric power generation system can work the self-contained wireless telemetry which is required a supplied voltage of at least 2.1V. On the other hand, the MPPT control method of photovoltaic power system is proposed [6]. This proposed method can achieve to track the maximum power point with only a single sensor. However, it is necessary that the generated power is calculated. These MPPT methods need a number of sensors and elaborate calculation.

This paper proposes a novel MPPT control method for thermoelectric power generation system of the constant load with only single current sensor. Estimating the output of the TM, the MPPT controller can track the maximum power point. Analyzing the thermoelectric power generation system with boost chopper by state space averaging method [7], the output of the TM estimates with only current sensor. The maximum power point voltage can be decided by both the estimated values and the internal resistance at the maximum power point. The proposed MPPT control method can achieve to track the maximum power point voltage without calculating the generated power of the TM. Digital computer simulation was implemented to demonstrate the validity and practicability of the proposed method using PSIM. Simulation results demonstrate that the proposed MPPT controller can track the maximum power point perfectly.

2. Characteristic of the Thermoelectric Power Module

In this paper, the six TMs (FPH1-12702AC), which consist of three series-connected TMs and two parallel-connected TMs is used. The cool side of the TM is set on a heat sink. The hot side of the TM is set on a tray with hot water. Figure 1 shows the V-I characteristics of the TM. We can see that the output power increases with rising temperature difference. Figure 2 shows the V-P characteristics of the TM. From Figure 2, we can see that the maximum power point voltage is changed by depending on the temperature difference.

Figure 1. V-I Characteristic of the thermoelectric module.
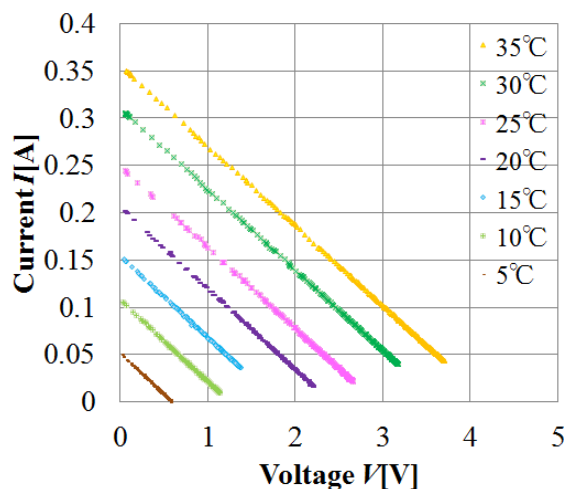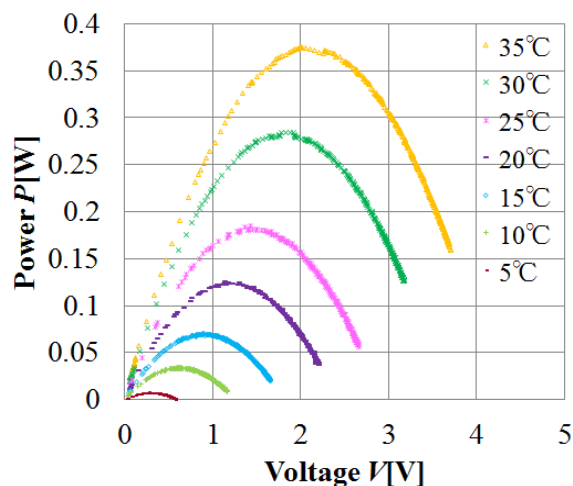

Figure 2. V-P Characteristic of the thermoelectric module.

We approximate the TMs for modeling on the PSIM. The output current I_T of the TM is approximated from Figure 1 as follows

$$I_T = -0.085V_T + 0.010\Delta T [\text{A}] \tag{1}$$

From Equation (1), the power *P* of the TM is given by

$$P = -0.085V_T^2 + 0.01\Delta T \cdot V_T [\text{W}] \tag{2}$$

At the maximum power point of Figure 2,

$$\frac{\partial P}{\partial V_T} = 0 \tag{3}$$

From Equation (3), the maximum power point voltage V_{Max} is given by

$$V_{Max} = 0.059 \Delta T [\text{V}] \tag{4}$$

From Equation (4) and Equation (1), V_{Max} is represented as follows

$$V_{Max} = 11.9 I_T \tag{5}$$

From this equation, the internal resistance R_M of the TM is 11.9 Ω at the maximum power point in this paper.

3. Proposed MPPT Control Method

Figure 3 shows the basic system configuration of the thermoelectric power generation system [3]. The thermoelectric power generation system uses a boost chopper because the load R_O which assumes the wireless telemetry is required a supplied voltage at least 2.1V. The input and output side of the boost chopper is connected the smoothing capacitors.

Figure 3. System configuration of the thermoelectric power generation system using a boost chopper.
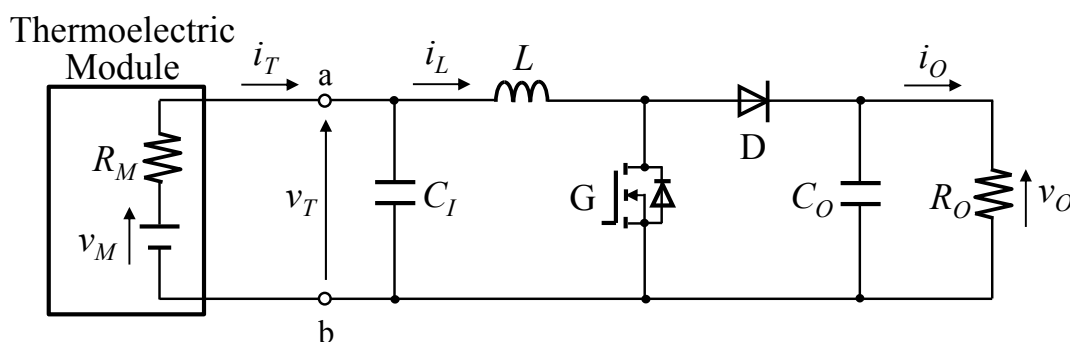
3.1. Analyzing the Thermoelectric Power Generation System

This section reveals that the output of the TM can estimate by using the linear analyzing result of the system. This paper uses the state space averaging method [7] for this analyzing. To reduce the power loss of the winding resistance of L, L is low inductance. On the other hand, R_O is the high impedance. As a result, the boost chopper acts in discontinuous current mode (DCM). There are three modes in DCM. Figure 4 illustrates the relationship between switching condition and i_L. D_1 is the duty ratio during G-on period, D_2 is the duty ratio during G-off and D-on period, D_3 is the duty ratio during G-off and D-off period. Thus, we analyze the three modes. Figure 5 shows the equivalent circuits of Figure 3. The state equations of Figure 5 set up where the state variable x is $(v_T \ i_L \ v_O)^T$.

Figure 4. Relationship between the switching condition and i_L.
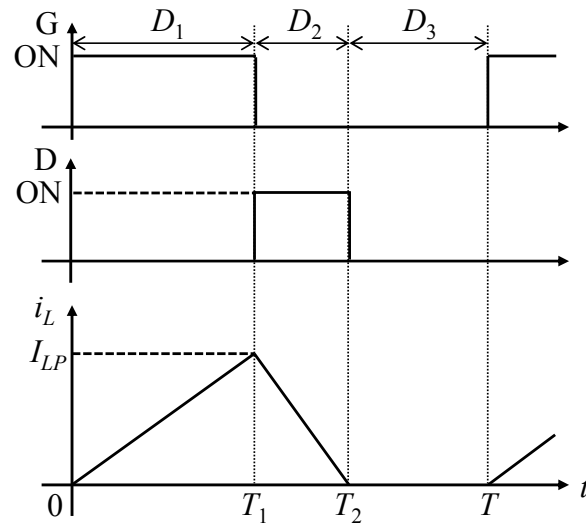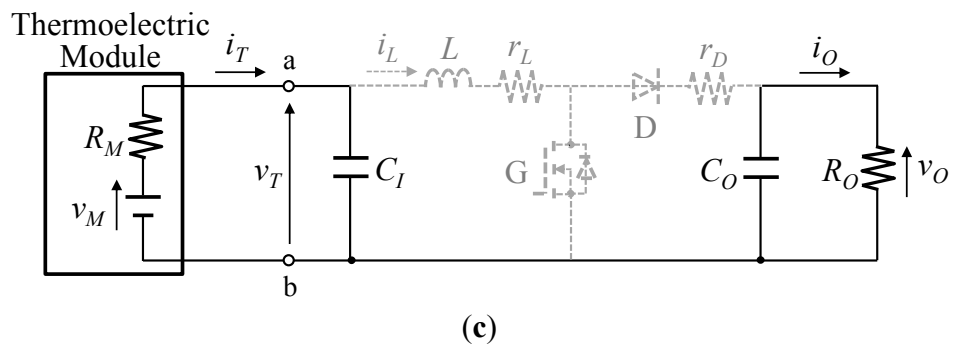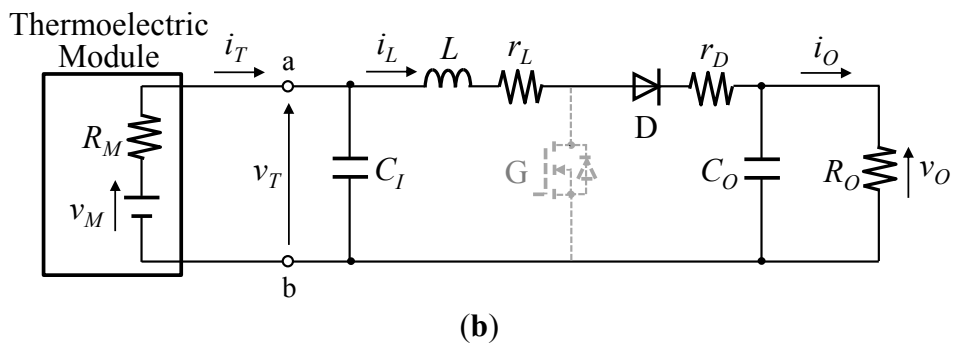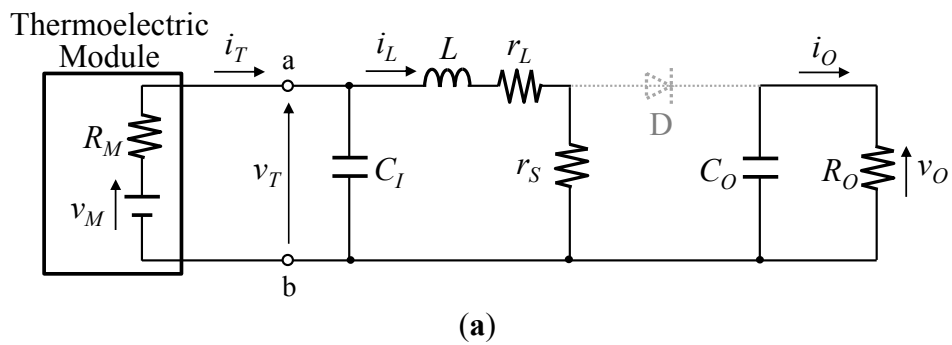

Figure 5. Equivalent circuits of the thermoelectric power generation system. (**a**) MODE 1; (**b**) MODE 2; (**c**) MODE 3.

(**a**)

(**b**)

(**c**)

During the MODE 1, the switch G is ON, and i_L increases from 0 to the peak value i_{LP}. Figure 5a illustrates the equivalent circuit in MODE 1. r_S is the ON-resistance of the MOSFET and r_L is the winding resistance of L. From Figure 5a, the state equation of the MODE 1 is given as follows

$$\frac{dv_T}{dt} = -\frac{v_T}{R_M C_I} + \frac{v_M}{R_M C_I} - \frac{1}{C_I} i_T \tag{6}$$

$$\frac{di_T}{dt} = \frac{v_T}{L} - \frac{r_L + r_s}{L} i_T \tag{7}$$

$$\frac{dv_O}{dt} = -\frac{v_O}{R_O C_O} \tag{8}$$

From these equations, the matrix is given by

$$\frac{d\mathbf{x}}{dt} = \mathbf{A_1 x} + \mathbf{b_1} V_M \tag{9}$$

where A_1 and b_1 are given by

$$\mathbf{A_1} = \begin{pmatrix} -\frac{1}{R_M C_I} & -\frac{1}{C_I} & 0 \\ \frac{1}{L} & -\frac{r_L + r_S}{L} & 0 \\ 0 & 0 & -\frac{1}{R_O C_O} \end{pmatrix}, \mathbf{b_1} = \begin{pmatrix} \frac{1}{R_M C_I} \\ 0 \\ 0 \end{pmatrix}$$

The switching time is very short. So, the right side of Equations (6), (7) and (8) are assumed the constant value. As a result, we approximate these equations as follows

$$\begin{aligned} v_T(D_1 T_s) - v_T(0) &= D_1 T_s \frac{dv_T}{dt}_{(t=0)} \\ &= -D_1 T_s \frac{v_T(0)}{R_M C_I} + D_1 T_s \frac{v_M(0)}{R_M C_I} - D_1 T_s \frac{i_T(0)}{C_I} \end{aligned} \tag{10}$$

$$\begin{aligned} i_T(D_1 T_s) - i_T(0) &= D_1 T_s \frac{di_T}{dt}_{(t=0)} \\ &= D_1 T_s \frac{v_T(0)}{L} - D_1 T_s \frac{r_L + r_s}{L} i_T(0) \end{aligned} \tag{11}$$

$$\begin{aligned} v_O(D_1 T_s) - v_O(0) &= D_1 T_s \frac{dv_O}{dt}_{(t=0)} \\ &= -D_1 T_s \frac{v_O(0)}{R_O C_O} \end{aligned} \tag{12}$$

During the MODE 2, the switch G is OFF, and the current flows into D. Figure 5b illustrates the equivalent circuit in MODE 2. r_D is the conduction resistance of D. From Figure 5b, the state equation of the MODE 2 is given as follows

$$\frac{dv_T}{dt} = -\frac{v_T}{R_M C_I} + \frac{v_M}{R_M C_I} - \frac{1}{C_I} i_T \tag{13}$$

$$\frac{di_T}{dt} = \frac{v_T}{L} - \frac{r_L + r_D}{L} i_T - \frac{1}{L} v_O \tag{14}$$

$$\frac{dv_O}{dt} = -\frac{i_T}{C_O} + \frac{v_O}{R_O C_O} \tag{15}$$

From these equations, the matrix is given by

$$\frac{d\mathbf{x}}{dt} = \mathbf{A}_2 \mathbf{x} + \mathbf{b}_2 V_M \tag{16}$$

where A_2 and b_2 are given by

$$\mathbf{A}_2 = \begin{pmatrix} -\frac{1}{R_M C_I} & -\frac{1}{C_I} & 0 \\ \frac{1}{L} & -\frac{r_L + r_D}{L} & -\frac{1}{L} \\ 0 & -\frac{1}{C_O} & -\frac{1}{R_O C_O} \end{pmatrix}, \mathbf{b}_2 = \begin{pmatrix} \frac{1}{R_M C_I} \\ 0 \\ 0 \end{pmatrix}$$

The right side of Equations (13), (14) and (15) are assumed the constant value. We approximate these equations as follows

$$v_T[(D_1 + D_2)T_s] - v_T(D_1 T_s) = -D_2 T_s \frac{v_T(0)}{R_M C_I} + D_2 T_s \frac{v_M(0)}{R_M C_I} - D_2 T_s \frac{i_T(0)}{C_I} \tag{17}$$

$$i_T[(D_1 + D_2)T_s] - i_T(D_1 T_s) = D_2 T_s \frac{v_T(0)}{L} - D_2 T_s \frac{r_L + r_s}{L} i_T(0) - D_2 T_s \frac{v_O(0)}{L} \tag{18}$$

$$v_O[(D_1 + D_2)T_s] - v_O(D_1 T_s) = -D_2 T_s \frac{i_T(0)}{C_O} + D_2 T_s \frac{v_O(0)}{R_O C_O} \tag{19}$$

During the MODE 3, $i_L = 0$. Figure 5c illustrates the equivalent circuit in MODE 3. From Figure 5c, the state equation of the MODE 3 is given as follows

$$\frac{dv_T}{dt} = -\frac{v_T}{R_M C_I} + \frac{v_M}{R_M C_I} \tag{20}$$

$$\frac{di_T}{dt} = 0 \tag{21}$$

$$\frac{dv_O}{dt} = \frac{v_O}{R_O C_O} \tag{22}$$

From these equations, the matrix is given by

$$\frac{d\mathbf{x}}{dt} = \mathbf{A}_3 \mathbf{x} + \mathbf{b}_3 V_M \tag{23}$$

where A_3 and b_3 are given by

$$\mathbf{A}_3 = \begin{pmatrix} -\frac{1}{R_M C_I} & 0 & 0 \\ 0 & 0 & 0 \\ 0 & 0 & -\frac{1}{R_L C_O} \end{pmatrix}, \mathbf{b}_3 = \begin{pmatrix} \frac{1}{R_M C_I} \\ 0 \\ 0 \end{pmatrix}$$

The right side of Equations (20), (21) and (22) are assumed the constant value. We approximate these equations as follows

$$v_T(T_s) - v_T[(D_1 + D_2)T_s] = -D_3 T_s \frac{v_T(0)}{R_M C_I} + D_3 T_s \frac{v_M(0)}{R_M C_I} \tag{24}$$

$$i_T(D_1 T_s) - i_T[(D_1 + D_2)T_s] = 0 \tag{25}$$

$$v_O(T_s) - v_O[(D_1 + D_2)T_s] = D_3 T_s \frac{v_O(0)}{R_O C_O} \tag{26}$$

Therefore, the difference equations in one switching cycle are given as follows

$$v_T(T_s) - v_T(0) = -\frac{v_T(0)}{R_M C_I} + \frac{v_M(0)}{R_M C_I} - (D_1 + D_2)\frac{i_T(0)}{C_I} \tag{27}$$

$$i_T(T_s) - i_T(0) = (D_1 + D_2)\frac{v_T(0)}{L} - D_1\frac{r_L + r_s}{L}i_T(0) - D_2\frac{r_L + r_D}{L}i_T(0) - D_2\frac{v_O(0)}{L} \tag{28}$$

$$v_O(T_s) - v_O(0) = -\frac{v_O(0)}{R_O C_O} - D_2\frac{i_T(0)}{C_O} \tag{29}$$

From these difference equations, the differential equations are given as follows:

$$\frac{dv_T}{dt} = -\frac{v_T(t)}{R_M C_I} + \frac{v_M(t)}{R_M C_I} - (D_1 + D_2)\frac{i_T(t)}{C_I} \tag{30}$$

$$\frac{di_T}{dt} = (D_1 + D_2)\frac{v_T(t)}{L} - D_1\frac{r_L + r_s}{L}i_T(t) - D_2\frac{r_L + r_D}{L}i_T(t) - D_2\frac{v_O(t)}{L} \tag{31}$$

$$\frac{dv_O}{dt} = -\frac{v_O(t)}{R_O C_O} - D_2\frac{i_T(t)}{C_O} \tag{32}$$

The averaging state vector is assumed as follows

$$\bar{\mathbf{x}} = \begin{pmatrix} \bar{v}_T & \bar{i}_L & \bar{v}_O \end{pmatrix}^T \tag{33}$$

The state averaging equation can be derived as

$$\frac{d\bar{\mathbf{x}}}{dt} = \mathbf{A}\bar{\mathbf{x}} + \mathbf{b}V_M \tag{34}$$

$$\mathbf{A} = \mathbf{A}_1 D_1 + \mathbf{A}_2 D_2 + \mathbf{A}_3 D_3$$

$$= \begin{pmatrix} -\frac{1}{R_M C_I} & -\frac{1}{C_I}D_{12} & 0 \\ \frac{1}{L}D_{12} & -\frac{r_L D_{12} + r_s D_1 + r_D D_2}{L} & -\frac{1}{L}D_2 \\ 0 & -\frac{1}{C_O}D_2 & -\frac{1}{R_O C_O} \end{pmatrix}$$

$$\mathbf{b} = \mathbf{b_1}D_1 + \mathbf{b_2}D_2 + \mathbf{b_3}D_3$$

$$= \begin{pmatrix} \dfrac{1}{R_M C_I} \\ 0 \\ 0 \end{pmatrix}$$

where $D_{12} = D_1 + D_2$. Equation (31) corresponds with Equations (27), (28) and (29). Therefore, the average value is derived from the parameters multiplied by the duty factors. The following equation can be written in the steady state

$$\frac{d\overline{\mathbf{x}}}{dt} = 0 \tag{35}$$

Therefore V_T, I_L and V_O in the steady state can be derived as

$$\begin{pmatrix} V_T \\ I_L \\ V_O \end{pmatrix} = \frac{V_M}{R_O D_2^2 + R_M D_{12}^2 + r_L D_{12} + r_S D_1 + r_D D_2} \cdot \begin{pmatrix} R_O D_2^2 + r_L D_{12} + r_S D_1 + r_D D_2 \\ D_{12} \\ R_O D_2 D_{12} \end{pmatrix} \tag{36}$$

The average value I_L of i_L is given as follows

$$I_L = \frac{D_{12}}{2} I_{LP} \tag{37}$$

where I_{LP} is the peak value of i_L [6]. The internal voltage V_M of the TM in the steady state is given by

$$V_M = \frac{I_L}{D_{12}} \left(R_O D_2^2 + R_M D_{12}^2 + r_L D_{12} + r_S D_1 + r_D D_2 \right) \tag{38}$$

The output voltage V_T of the TM can be derived as

$$V_T = \frac{I_L}{D_{12}} \left(R_O D_2^2 + r_L D_{12} + r_S D_1 + r_D D_2 \right) \tag{39}$$

The output current I_T of the TM can be expressed as

$$I_T = \frac{V_M - V_T}{R_M} \tag{40}$$

Therefore V_M, V_T and I_T can be estimated by detecting the inductor current i_L and the duty ratio.

3.2. Proposed MPPT Control Method

Figure 6 shows the circuit diagram using the proposed MPPT control method. The peak value i_{LP} yields by using the peak hold circuit of i_L. V_T and I_T can be estimated by Equations (36) and (37). The impedance matching condition is to match v_T to the voltage of R_M. The reference value of the boost chopper is given by

$$V_{ref}^* = I_T R_M \tag{41}$$

The PI controller uses to track the reference and reduce the error, which is obtained by subtracting V_T from V^*_{ref} close to zero. The duty ratio D_1 of the MODE 1 is calculated by the output value v_C of the PI controller. The duty ratio D_2 of the MODE 2 is calculated by the discontinuous period of i_L and D_1.

Figure 6. A circuit diagram with the proposed MPPT control method.
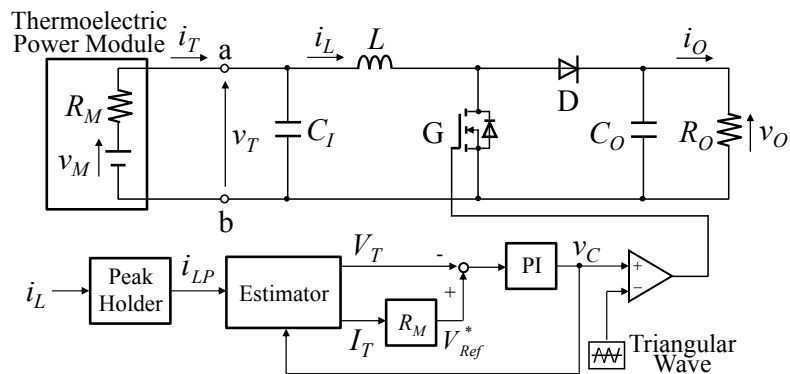
Thus the MPPT control method in this paper can be estimated the output of the TM with only current sensor by analyzing the boost chopper using state space averaging method. The internal resistance of the TM is constant at the maximum power point whether the temperature difference or not. Hence, the voltage of the maximum power point can be decided without calculation of the power.

4. Simulation Results

Digital computer simulation using PSIM software is implemented to confirm the validity and practicability of the proposed MPPT control method. The TM is demonstrated current source in PSIM software, where the output of the current source is decided by Equation (1).

Table 1 indicates the circuit constants of Figure 6. The carrier frequency is 7.81 kHz. The low-pass filter of the input side of the boost chopper consists of the input capacitor C_I and the internal resistance R_M. The cut-off frequency f_c is given by

$$f_c = \frac{1}{2\pi R_M C_I} [\text{Hz}] \tag{42}$$

In this paper, the cut-off frequency f_c is about 160 Hz. This simulation allows for the winding resistance of L, the ON resistance of D and the switch G in the experimental setup [3]. The proportional gain K is 0.1 and the integral time T_I is 0.01s in the PI controller.

Table 1. Circuit parameters of the thermoelectric power generation system.

Parameter	Symbol	Value
Input capacitor	C_I	100 μF
Inductor	L	150 μH
Output capacitor	C_O	1000 μF
Load resistor	R	1 kΩ
Winding resistor of the inductor L	r_L	0.26 Ω
Conduction resistance of the diode D	r_D	0.1 Ω
ON-resistance of the MOSFET	r_S	8.5 mΩ

Figure 7. Simulation results by using the proposed MPPT control when the thermal difference is 35 °C. (**a**) During the starting period; (**b**) Magnified waveforms in the vicinity of 3.0 s.
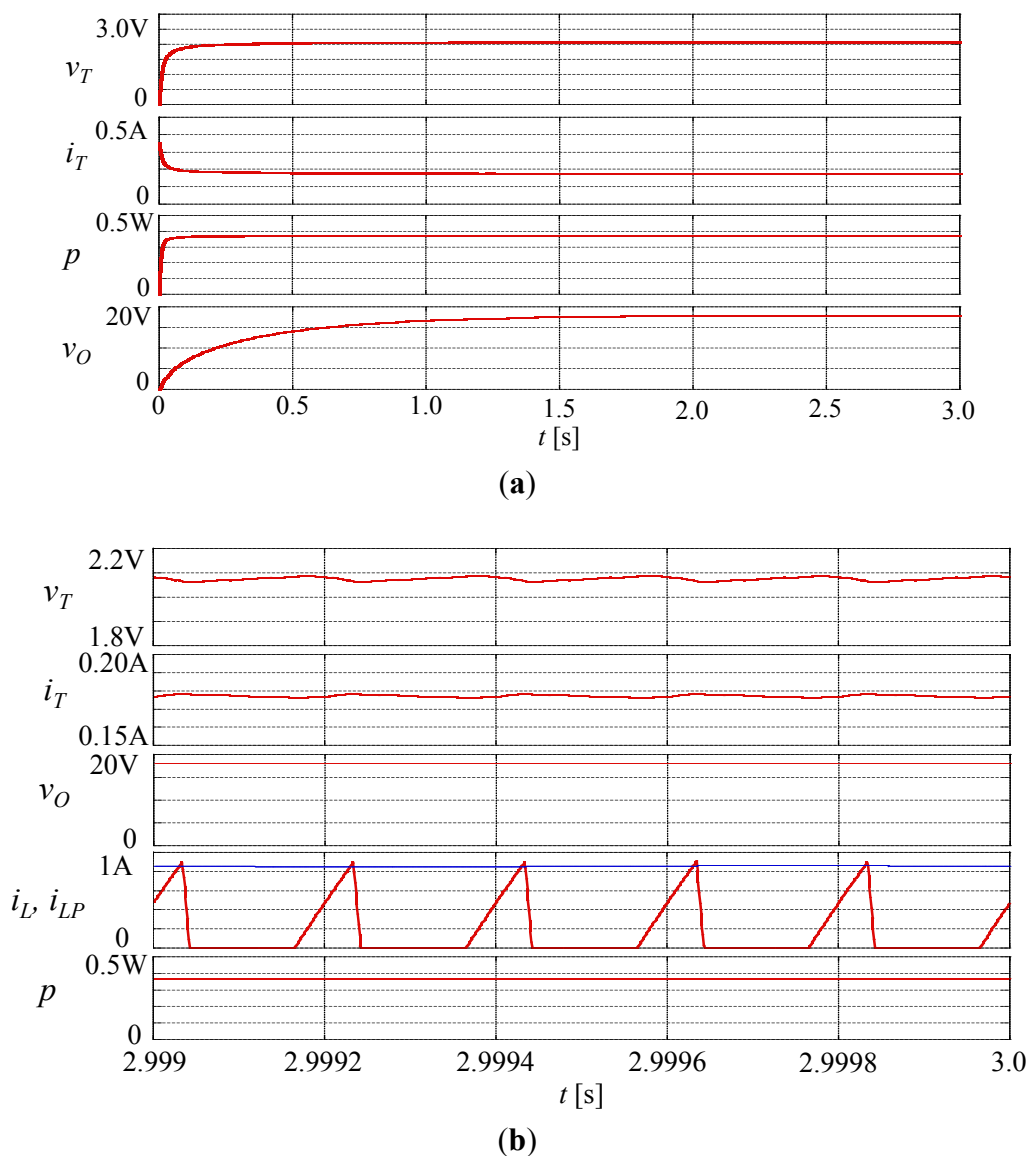

(**a**)

(**b**)

Figure 7 shows the simulation results of the proposed MPPT control method at $\Delta T = 35$ °C. Figure 7a is the simulation waveforms during the starting period. Figure 7b is the magnified waveforms in the vicinity of 3.0 s in Figure 7a. v_T is the output voltage of the TM, i_T is the output current of the TM, p is the output power of the TM, v_O is the load voltage, i_L is the inductor current and i_{LP} is the value of the peak holder. The peak holder tracks the peak value of i_L. v_T is 2.0V in the steady state. This result agrees well with the Equation (4).

This paper implements the simulation by using the conventional hill-climb method. Figure 8 shows the simulated results of the hill-climb method at $\Delta T = 35$ °C. Figure 8a is the simulation waveforms during the starting period. Figure 8b is the magnified waveforms in the vicinity of 3.0 s in Figure 8a. From these simulation, v_T is 1.9V in the steady state. This result agrees well with the Equation (4). And then, the performance of the proposed MPPT control method corresponds with the conventional hill-climb method.

Figure 8. Simulated results by using the conventional hill-climb method when the thermal difference is 35 °C. (**a**) During the starting period; (**b**) Magnified waveforms in the vicinity of 3.0 s.
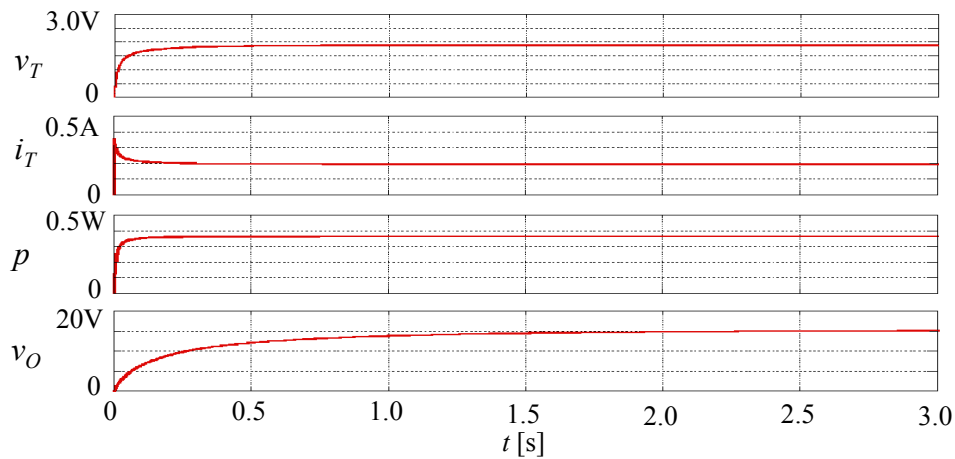

(**a**)
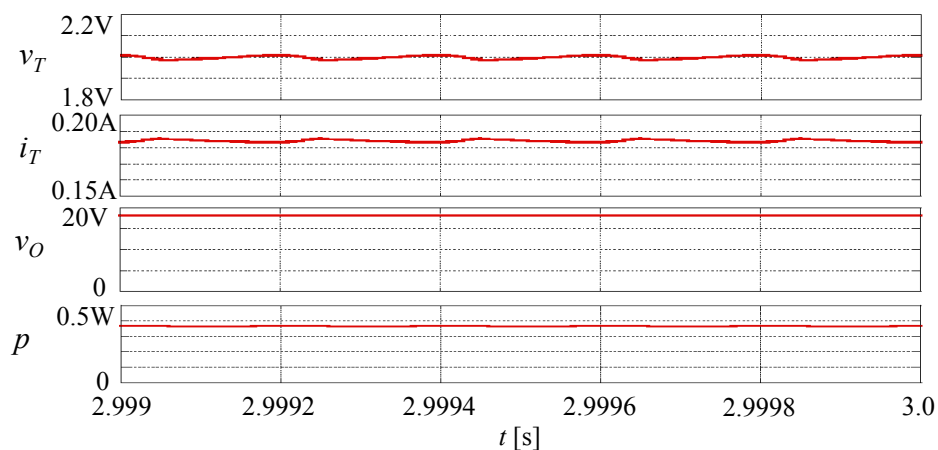
(**b**)

Figure 9 shows the simulation results in the case of the thermal difference fluctuation. ΔT is the temperature difference waveform. We assume that ΔT is the ramp reference. Although the thermal difference changes 7 °C/s, v_T is tracked the maximum power point voltage by the proposed MPPT controller. The thermoelectric power generation system with the proposed MPPT controller can harvest the maximum power regardless of the temperature variation perfectly.

Figure 10 shows the simulation results of V_T and p relative to approximation formulas. From Figure 9a, it can be seen that the average value of v_T agrees well with Equation (4). And then, it can be seen that the average value of p agrees very well with Equation (2). From these results, the proposed MPPT controller can harvest the maximum power of the TM.

Figure 9. Simulation results in the case of the thermal difference fluctuation. (**a**) From 0 to 35 °C; (**b**) From 35 °C to 0.
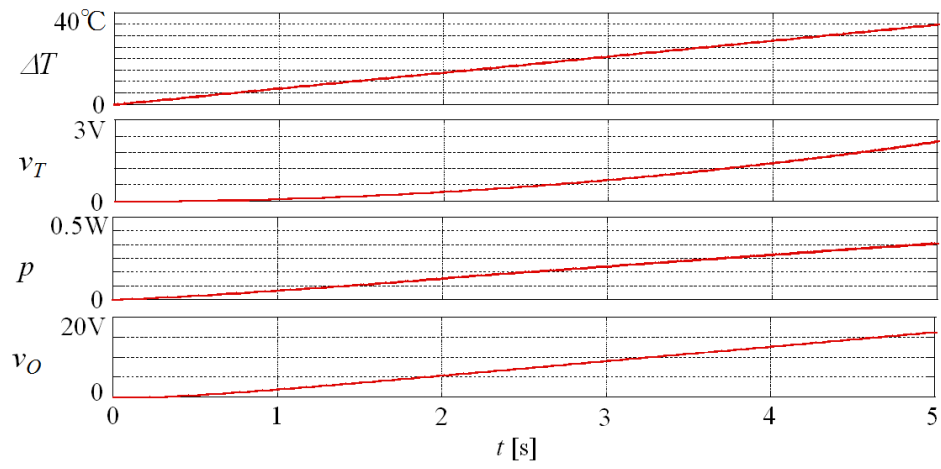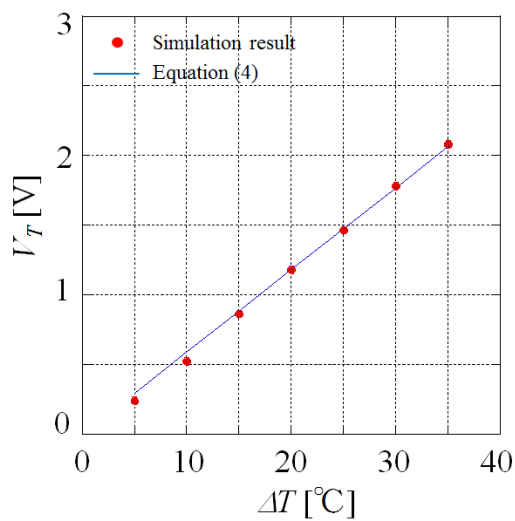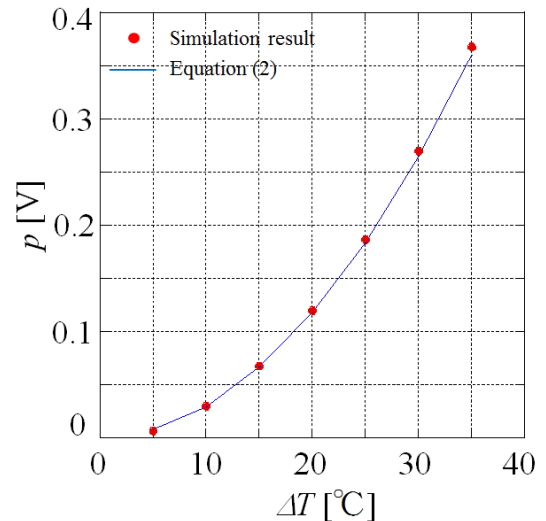

(**a**)
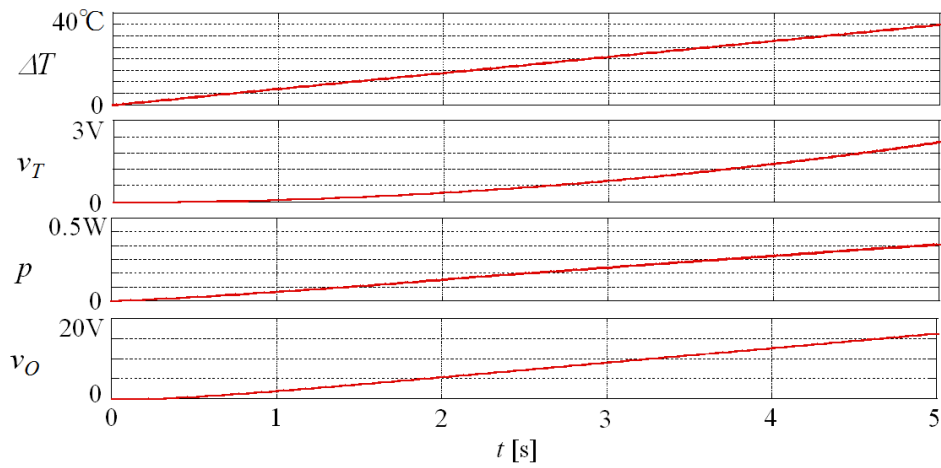
(**b**)

Figure 10. Simulation results of V_T and p relative to approximation formulas. (**a**) ΔT-V_T; (**b**) ΔT-p.

(**a**)

(**b**)

5. Conclusions

This paper proposed a novel MPPT control method for thermoelectric power generation using the state space averaging method. Estimating the output of the TM with only a current sensor, the MPPT controller can track the maximum power point. In the proposed method, the maximum power point voltage can be decided by the estimated values and the internal resistance at the maximum power point.

This paper revealed the electric characteristics and internal resistance of the TM. Analyzing the thermoelectric power generation system with boost chopper by state space averaging method, the output voltage and current of TM were estimated with only single current sensor. The maximum power point voltage can track without calculating the output power of the TM. Digital computer simulation was implemented to demonstrate the validity and practicability of the proposed method using PSIM. From the simulation results, the output power was about 0.36 W with the proposed MPPT control method when the temperature difference was 35 °C. Simulation results demonstrate that the proposed MPPT controller can track the maximum power point regardless of the temperature variation perfectly.

References

1. Singh, B.; Tan, L.; Date, A.; Akbarzadeh, A. Power Generation from Salinity Gradient Solar Pond Using Thermoelectric Generators for Renewable Energy Application. In Proceeding of the 2012 IEEE International Conference on Power and Energy (PECon), Kota Kinabalu, Malaysia, 2–5 December 2012; pp. 89–92.
2. Ishiyama, T.; Takahashi, T.; Yamada, H. Energy Harvesting Technology for Self-contained Wireless Telemetry Using Thermoelectric Generators. In Proceeding of the 16th International Conference on Electrical Engineering, Busan, Korea, 11–14 July 2010.
3. Ishiyama, T.; Yamada, H. Effect of Heat Pipes to Suppress Heat Leakage for Thermoelectric Generator of Energy Harvesting. In Proceeding of the 2012 International Conference on Renewable Energy Research and Applications (ICRERA), Nagasaki, Japan, 11–14 November 2012; pp. 1–4.
4. He, H.; Nagayoshi, H.; Kajikawa, T. A Method of Maximum Power Point Tracking of Thermoelectric Power Generation. In Proceeding of the IEEJ Power and Energy National Conference, Tokyo, Japan, 6–8 August 2003; pp. 465–466.
5. Yamada, H.; Hanamoto, T.; Ishiyama, T.; Sakaguchi, T.; Takahashi, T. A novel MPPT control method for thermoelectric generation by temperature detection. *J. Jpn Inst. Power Electron.* **2011**, *36*, 151–157.
6. Noguchi, T.; Matsumoto, H. Maximum-Power-Point Tracking Method of Photovoltaic Power System. *IEEJ Trans. IA.* **2005**, *125*, 54–59.
7. Harada, K.; Ninomiya, T.; Gu, B. The fundamentals of switched-mode converters. *Corona Publ.* **1992**, 65–71.